Chemistry–A European Journal
Research Article
doi.org/10.1002/chem.202103761
Chemistry Europe
European Chemical Societies Publishing
www.chemeurj.org

Solvothermal Synthesis of $[Cr_7S_8(en)_8Cl_2]Cl_3 \cdot 2H_2O$ with Magnetically Frustrated $[Cr_7S_8]^{5+}$ Double-Cubes**

Eranga H. Gamage,[a, b] Judith K. Clark,[c] Maher Yazback,[d] Hai-Ping Cheng,[d] Michael Shatruk,[c, e] and Kirill Kovnir*[a, b]

Abstract: A novel transition metal chalcohalide $[Cr_7S_8(en)_8Cl_2]Cl_3 \cdot 2H_2O$, with $[Cr_7S_8]^{5+}$ dicubane cationic clusters, has been synthesized by a low temperature solvothermal method, using dimethyl sulfoxide (DMSO) and ethylenediamine (*en*) solvents. Ethylenediamine ligand exhibits bi- and monodentate coordination modes; in the latter case ethylenediamine coordinates to Cr atoms of adjacent clusters, giving rise to a 2D polymeric structure. Although magnetic susceptibility shows no magnetic ordering down to 1.8 K, a highly negative Weiss constant, $\theta = -224(2)$ K, obtained from Curie-Weiss fit of inverse susceptibility, suggests strong antiferromagnetic (AFM) interactions between $S = 3/2$ Cr(III) centers. Due to the complexity of the system with $(2S+1)^7 = 16384$ microstates from seven Cr^{3+} centers, a simplified model with only two exchange constants was used for simulations. Density-functional theory (DFT) calculations yielded the two exchange constants to be $J_1 = -21.4$ cm^{-1} and $J_2 = -30.2$ cm^{-1}, confirming competing AFM coupling between the shared Cr^{3+} center and the peripheral Cr^{3+} ions of the dicubane cluster. The best simulation of the experimental data was obtained with $J_1 = -20.0$ cm^{-1} and $J_2 = -21.0$ cm^{-1}, in agreement with the slightly stronger AFM exchange within the triangles of the peripheral Cr^{3+} ions as compared to the AFM exchange between the central and peripheral Cr^{3+} ions. This compound is proposed as a synthon towards magnetically frustrated systems assembled by linking dicubane transition metal-chalcogenide clusters into polymeric networks.

Introduction

Transition metals in combination with group 13–16 elements are known to form polyhedral clusters that are worth exploring owing to their numerous applications in catalysis and photovoltaics.[1,2] Hollow coordination cages made of transition metals and organic bridging ligands have triggered much interest in the scientific community due to their host-guest chemistry.[3,4] Among these diverse polyhedral types, inorganic-organic hybrid compounds made of single cuboidal cores are the most extensively studied due to their magnetic, optical, photophysical, and stereochemical properties.[5,6] Eight-vertex Sn_4O_4 clusters chelated by phosphinate ligands catalyze a range of organic interconversions.[7,8] Transition metal catalysts based on Co_4O_4 cubane clusters were reported to catalyze the oxidation of organic substrates.[9] The cubane-like core is the universal motif of all photosynthetic enzymes responsible for photocatalytic water splitting in the oxygen evolving complexes in green plants.[10] In fact, many theoretical investigations have been conducted to understand the mechanism behind diverse roles played by these ubiquitous clusters.[11–13] Enzymes that resemble the iron-sulfur clusters, Fe_4S_4, present in the active sites of photosystems have been extensively used in biomimetic inorganic chemistry.[14] The Fe_4S_4 cubane clusters have been also exploited in the catalytic chalcogel frameworks for the commercial production of hydrogen.[15,16]

Cuboidal structures containing magnetic cations arranged in a tetrahedral geometry (in the alternating corners of the

[a] E. H. Gamage, Prof. Dr. K. Kovnir
Department of Chemistry
Iowa State University
Ames, Iowa 50011 (USA)
[b] E. H. Gamage, Prof. Dr. K. Kovnir
Ames Laboratory, U.S. Department of Energy
Ames, Iowa 50011 (USA)
E-mail: kovnir@iastate.edu
[c] J. K. Clark, Prof. Dr. M. Shatruk
Department of Chemistry and Biochemistry
Florida State University, Tallahassee
Florida 32306 (USA)
[d] M. Yazback, Prof. Dr. H.-P. Cheng
Department of Physics
Center for Molecular Magnetic Quantum Materials
and Quantum Theory Project
University of Florida
Gainesville, Florida 32611 (USA)
[e] Prof. Dr. M. Shatruk
National High Magnetic Field Laboratory
Tallahassee, Florida 32310 (USA)

[**] *en* = ethylenediamine.

Supporting information for this article is available on the WWW under https://doi.org/10.1002/chem.202103761

cube) allow antiparallel spin pairing that leads to magnetic frustration. Magnetostructural correlations in complexes with a M_4O_4 (M = metal) cubane-type core have been under study for several decades. Density functional theory (DFT) calculations conducted on the compounds containing a Cu_4O_4 core have revealed a competition between ferromagnetic (FM) and antiferromagnetic (AFM) coupling through Cu–O bonds.[17] Magnetic properties of Fe_4O_4 cubane clusters have been tuned via the control of the ligands, such as μ-oxo bridges of N_4O pentadentate ligands affecting the structure and properties of the iron-alkoxide cubane-like Fe_4O_4 complexes.[18] In alkoxo-bridged Ni_4O_4 cube structures, switching of the ground spin state has been observed based on the solvent-induced differences in the structural arrangement.[19]

The complexity of the cubane-core clusters can be raised by fusing two cubane units via a common metal vertex. Besides oxo-dicubanes, such as $Co_7(\mu_3\text{-}OH)_8$,[20] chalcogenide dicubanes have been intensively studied. Main group element chalcogenide dicubanes are explored for their non-linear optical ($[Sb_7Ch_8]^{5+}$ and $[Sb_7Ch_8X_2]^{3+}$, Ch: chalcogen; X: halogen)[21–24] and catalytic (Sn_7S_8)[25] properties. Many single and double cuboidal derivatives of molybdenum chalcogenides have been exploited to understand the metal-metal bonding in different cluster types.[26–30] Double-cubane type copper complexes with exogenous anions showed strong AFM coupling between Cu(II) centers with reduced magnetic moments as a result of magnetic exchange facilitated by their topology and connectivity.[31–33] In contrast, Cr-containing dicubanes are much less studied. There are only two structural reports of Cr(III) complexes that contain $[Cr_7S_8]^{5+}$ dicubane cations bound to simple monodentate ligands.[34,35] Here we report synthesis, crystal structure, and detail analysis of magnetic properties for a novel dicubane cluster, $[Cr_7S_8(en)_8Cl_2]Cl_3\cdot 2H_2O$ (*en*: ethylenediamine). We demonstrate that this compound exhibits strong magnetic frustration due to the similarity of the distances and AFM exchange coupling constants between the Cr^{3+} vertices of the dicubane unit.

Experimental Section

Synthesis: Starting materials were used as received. $[Cr_7S_8(en)_8Cl_2]Cl_3\cdot 2H_2O$ phase was first synthesized by a solvothermal reaction of 1 mmol of $CrCl_3\cdot 6H_2O$ (Alfa Aesar, 98%) with 1 mmol of dimethyl sulfoxide (DMSO, Alfa Aesar, 99+%) in 8 mL of ethylenediamine (Alfa Aesar, 99%) at 200 °C for 3–5 days in a 46 mL Teflon-lined stainless-steel autoclave. The filling fraction of the Teflon liner for the reaction was ~17%. Once the reaction was completed, the autoclave was taken out of the furnace and naturally cooled to room temperature. The resultant solid was filtered and washed with aliquots of absolute ethanol. The product contained shiny black block-like crystals (Figure S1) which were used for crystal structure determination by single crystal X-ray diffraction. Powder X-ray diffraction (PXRD) patterns of the bulk samples contained some unidentified peaks which did not belong to any known binary chromium selenides. The yield of $[Cr_7S_8(en)_8Cl_2]Cl_3\cdot 2H_2O$ phase increased with increasing concentration of DMSO used (Figure S2). When the amount of DMSO was increased to 5 mmol, under the same reaction conditions, a phase-pure $[Cr_7S_8(en)_8Cl_2]Cl_3\cdot 2H_2O$ was obtained. Addition of aliquots (5 mmol) of distilled water to the reaction medium helped in obtaining better quality crystals. All syntheses were conducted under ambient conditions due to the air and moisture stability of the title compound. A fine powder sample obtained by grinding the crystals was utilized for magnetic property measurements.

Characterization: PXRD patterns of finely ground crystals were acquired on a bench-top Rigaku 600 Miniflex X-ray diffractometer with a Cu-K_α radiation (λ = 1.54185 Å) and a Ni-K_β filter. Single crystal X-ray diffraction experiment was performed by mounting a single crystal of $[Cr_7S_8(en)_8Cl_2]Cl_3\cdot 2H_2O$ on a cryoloop that was placed on a goniometer of a Bruker D8 Venture diffractometer with a Photon100 CMOS detector and Mo-K_α radiation source (λ = 0.71073 Å). The crystal was cooled to 100 K under a constant flow of dry N_2. Data reduction and crystal structure solution and refinement were performed using APEX3 and SHELX software packages.[36,37]

Magnetic measurements were conducted on ~5.6 mg of powdered crystals of $[Cr_7S_8(en)_8Cl_2]Cl_3\cdot 2H_2O$, using a Magnetic Property Measurements System, MPMS-XL (Quantum Design), equipped with a superconducting quantum interference device (SQUID). Temperature dependence of magnetic susceptibility (χ vs. T) was studied in the applied magnetic field of 1000 Oe, and the Curie-Weiss fitting of $1/\chi$ vs. T was performed in the temperature range of 100–300 K. Isothermal field dependence of magnetization (M vs. H) was studied in a varying field of 0–70 kOe at 1.8 K. The data were corrected for the diamagnetic contribution from the sample holder and for the intrinsic diamagnetism of the material. To obtain the values of the exchange coupling constants, J, the magnetic data were simulated with the Magpack software.[38]

SEM images of bead-like crystals of $[Cr_7S_8(en)_8Cl_2]Cl_3\cdot 2H_2O$ were obtained by mounting crystals onto graphite tape. Elemental analysis was conducted on these crystals and the data were analyzed for chemical composition using Aztec software. Getting accurate statistics was challenging due to heavy charging of the sample. Fast acquisition (~few seconds) had to be done to prevent charging particles reaching the detector which resulted in poor data-to-noise ratios. The refined composition of heavy atoms normalized per 7 Cr atoms was $Cr_7S_{7.8(4)}Cl_{1.8(6)}$ which underestimates the Cl composition in 7:8:5 ratio determined by single-crystal X-ray diffraction. Variable pressure low vacuum technique was employed to reduce charging by maintaining the chamber pressure at 40 Pa using He gas. The normalized composition thus obtained was $Cr_7S_{7.8(4)}Cl_{2.7(1)}$ which still underestimates the Cl content due to substantial charging of particles. Other attempts of measuring such as using a cold-pressed 10 mm pellet prepared from finely ground crystals or coating the sample with a thin layer of Rh metal to minimize charging resulted in similar underestimation of Cl content.

Bulk chemical analysis of chloride was performed by means of standard gravimetric analysis method. 70 mg (0.0532 mmol) of $[Cr_7S_8(en)_8Cl_2]Cl_3\cdot 2H_2O$ were completely dissolved in 50 mL of 50% dilute HNO_3 (Fischer Chemicals) upon continuous stirring at 50 °C. About 1.5 g (8.83 mmol) of $AgNO_3$ (Fischer Chemicals, 100%) was added to this mixture which instantly formed the cloudy white precipitate AgCl. Contents were filtered and washed with distilled water followed by washing with acetone. The solid product was completely dried before recording the mass which came out to be 37.6 mg (0.262 mmol). Thus, one mole of the studied material contains 4.92 moles of Cl which is close to the expected composition of 5 Cl.

Thermal decomposition studies on $[Cr_7S_8(en)_8Cl_2]Cl_3\cdot 2H_2O$ were conducted at the beamline 17-BM–B (λ = 0.24075 Å) at the Advanced Photon Source, Argonne National Laboratory. Roughly a

2 mm column of finely ground sample was loaded at the center a capillary (0.9 mm ID and 1.1 mm OD) and was sandwiched between two silica wool plugs. The capillary was mounted horizontally on to the flow cell in a manner that the thermocouple barely touched the silica wool plug from the open end, and the X-ray beam is aimed at the center of the solid. The sample was heated in air from 25–450 °C using a heating profile and temperature dependent *in-situ* PXRD patterns were obtained simultaneously while oscillating the capillary 0.5 mm from the center. The sample was thermally stable until ~340 °C and started gradually decomposing afterwards as evidenced by the decreasing intensity of diffraction peaks (Figure S3). The phase becomes completely amorphous or decomposed/melted by ~380 °C as verified by the absence of diffraction peaks. It neither transformed into any Cr–S binary phase nor formed chromium oxides. Similar *ex-situ* decomposition studies were conducted in the laboratory using a flow furnace under a constant N_2 flow, and similar thermal stability range was observed. The observed amorphization was reversible, i.e., a solvothermal treatment of the sample decomposed at ~380 °C, using conditions identical to original synthesis (DMSO + ethylenediamine at 200 °C in the presence of NH_4Cl) produced the original crystalline $[Cr_7S_8(en)_8Cl_2]Cl_3 \cdot 2H_2O$ phase.

Quantum-mechanical calculations: First-principles calculations were performed with the Vienna *ab initio* Simulation Package (VASP)[39,40] within the density functional theory (DFT) framework.[41] Projector augmented wave pseudopotentials[42] and the generalized gradient approximations (GGA) of Perdew, Burke, and Ernzerhof[43] were used for the exchange-correlation energy. To approximate the on-site Coulomb interaction of Cr(*3d*) electrons, we apply the $+U$ method with a value of $U = 1$ eV. Wavefunctions were expanded in plane waves and an energy cutoff of 560 eV was used for all calculations. The Brillouin zone the of unit cell was sampled using a $2\times2\times2$ gamma centered *k*-mesh with the Gaussian smearing method. The experimental atomic structure and unit cell parameters were used for all calculations.

Results and Discussion

Synthesis

DMSO is a widely used sulfoxide ligand in the synthesis of platinum and palladium containing catalysts for aerobic oxidation.[44,45] It has also been utilized as an ambidentate ligand in coordination chemistry due to its μ-DMSO-*S*,*O* coordination mode apart from monodentate –*O* and –*S* modes.[46,47] Apart from this, *Kogan* et al. investigated its applicability as a bridging ligand to facilitate exchange interactions between transition metal centers in binuclear complexes.[48] However, employing DMSO as a potential sulfur source is rare in solution chemistry. About a decade ago, *Li* et al. synthesized an organic intercalated iron sulfide layered semiconductor using DMSO as a starting material without using elemental sulfur or thiourea.[49] Inspired by this work, we have successfully synthesized a couple of chromium sulfide compounds (including this work) following the same approach. Even though the mechanism of formation is not established yet, we can assume ethylenediamine, which is the solvent in the aforementioned synthesis, to play a role in breaking down DMSO and reducing sulfur to S^{2-} to react with the transition metal cations.[50] Based on this work, we can confidently declare DMSO as a suitable sulfur source which might help with the synthesis of other S-containing compounds in coordination chemistry.

Crystal structure

$[Cr_7S_8(en)_8Cl_2]Cl_3 \cdot 2H_2O$ crystallizes in a triclinic space group $P\bar{1}$ (Table 1). It has a polymeric structure with $[Cr_7S_8]^{5+}$ double-cubane type clusters as the primary building units. Cr and S atoms alternate in the corners of the cubes. The Cr1 atom occupying the 1 *h* site ($\bar{1}$; $^1/_2,^1/_2,^1/_2$) is shared between the two

Table 1. Data collection and structure refinement parameters with some selected interatomic distances for $[Cr_7S_8(en)_8Cl_2]Cl_3 \cdot 2H_2O$. Deposition number 2116011 contains the supplementary crystallographic data for this paper. These data are provided free of charge by the joint Cambridge Crystallographic Data Centre and Fachinformationszentrum Karlsruhe Access Structures service.

Data collection and refinement details		Atoms	Distance [Å]
crystal description	black beads	Cr1-S1	2.446(1)
temperature [K]	100(2)	Cr1-S2	2.435(2)
λ [Å]	Mo-K_α 0.71073	Cr1-S4	2.405(2)
crystal system	Triclinic	Cr2-S1	2.359(2)
space group	$P\bar{1}$ (No. 2)	Cr2-S3	2.396(2)
a [Å]	10.522(3)	Cr2-S4	2.342(1)
b [Å]	10.546(3)	Cr3-S1	2.351(2)
c [Å]	12.106(3)	Cr3-S2	2.377(1)
α [°]	90.596(2)	Cr3-S3	2.397(2)
β [°]	101.020(2)	Cr4-S2	2.387(2)
γ [°]	116.192(2)	Cr4-S3	2.369(1)
V [Å^3]	1176.4(6)	Cr4-S4	2.368(2)
Z	1	Cr4-Cl1	2.455(2)
formula weight [g mol^{-1}]	1314.57	**D-H····A**	**H····A [Å]**
ρ_{calc} [g cm^{-3}]	1.86	N–H····Cl	2.25(1)-2.85(1)
μ [mm^{-1}]	2.237	N–H····O	2.42(1)
data/parameters	4600/253	N–H····S	2.37(1)–2.77(1)
R_1/wR_2	0.045/0.092	O–H····Cl	2.31(3)
GOF	1.026	O–H····S	2.68(5)
difference peak/hole [e·Å^3]	0.83/-0.65	O–H····O	2.71(8)

$[Cr_4S_4]$ cubes to form a centrosymmetric double-cubane cluster (Figure 1A). Thus, the Cr1 atom is coordinated by six μ_3-S atoms, three from each cube. The Cr–S bond lengths vary in a range of 2.342(1) Å - 2.446(1) Å (Table 1), while ∡Cr–Se-Cr and ∡Se–Cr-Se angles vary from 87.03(5)° to 92.32(5)°. Ethylenediamine molecules bind to Cr atoms in two different coordination modes, either monodentate or bidentate, to complete the octahedral geometry. Cr2/Cr3 atoms connect to three S atoms, one bidentate-*en* and one monodentate-*en* molecules, while Cr4 atoms bind to three S atoms, one Cl atom and one bidentate-*en* molecule completing the distorted octahedral geometry around Cr centers (Figure 1B). This coordination gives rise to the $[Cr_7S_8(en)_8Cl_2]^{3+}$ cationic units. Additional charge balancing Cl^- anions occupy the vertices of the unit cell (Figure 1C). Cr–N bond distances span a range of 2.099(3) Å–2.176(5) Å (Table S1).

Ethylenediamine molecules play an important role in the orientation and packing of the overall structure. The linker *en* molecules connect Cr2/Cr3 atoms of adjacent clusters in a diagonal fashion along the [001] direction (Figure 1C), creating a 2D polymeric structure. Channels of well separated double cubane cationic clusters linked by *en* molecules extend along [010] direction (Figure 1C). Space filling water molecules are arranged in the vicinity of the C–C bonds of linker *en* molecules. The three-dimensional supramolecular structure of $[Cr_7S_8(en)_8Cl_2]Cl_3\cdot 2H_2O$ is further supported by a network of hydrogen bonds between NH_2 groups of *en* ligands, H_2O molecules, and Cl anions. The hydrogen bond lengths extend across 2.25(1)–2.85(1) Å (Table 1; donor: D and acceptor: A).

In the previously reported $[Cr_7S_8(SCN)_4(NH_3)_{14}](SH)$ double-cube type compound, composed of isolated $[Cr_7S_8(SCN)_4(NH_3)_{14}]^+$ cationic clusters accompanied by $(HS)^-$ anions, the clusters were connected only by weak $NH_3\cdots S$ and $NH_3\cdots SCN^-$ hydrogen bonds.[34] Another reported Cr dicubane, chalcohalide $[Cr_7S_8Cl_2(NH_3)_{14.5}(H_2O)_{1.5}]Cl_3\cdot H_2O$, also contains isolated $[Cr_7S_8Cl_2(NH_3)_{14.5}(H_2O)_{1.5}]^{3+}$ cations and Cl^- anions linked via different hydrogen bonding interactions: N–H···Cl, N–H···O, O–H···Cl and O–H···S.[35] Since none of the reported examples of Cr–S dicubanes has clusters interconnected by covalent bonds forming a polymeric structure, to the best of our knowledge, the title compound is the first ever $[Cr_7S_8]^{5+}$ double-cubane compound of polymeric nature.

Magnetic properties

Magnetic measurements were conducted on a polycrystalline sample of $[Cr_7S_8(en)_8Cl_2]Cl_3\cdot 2H_2O$ obtained by finely grinding a

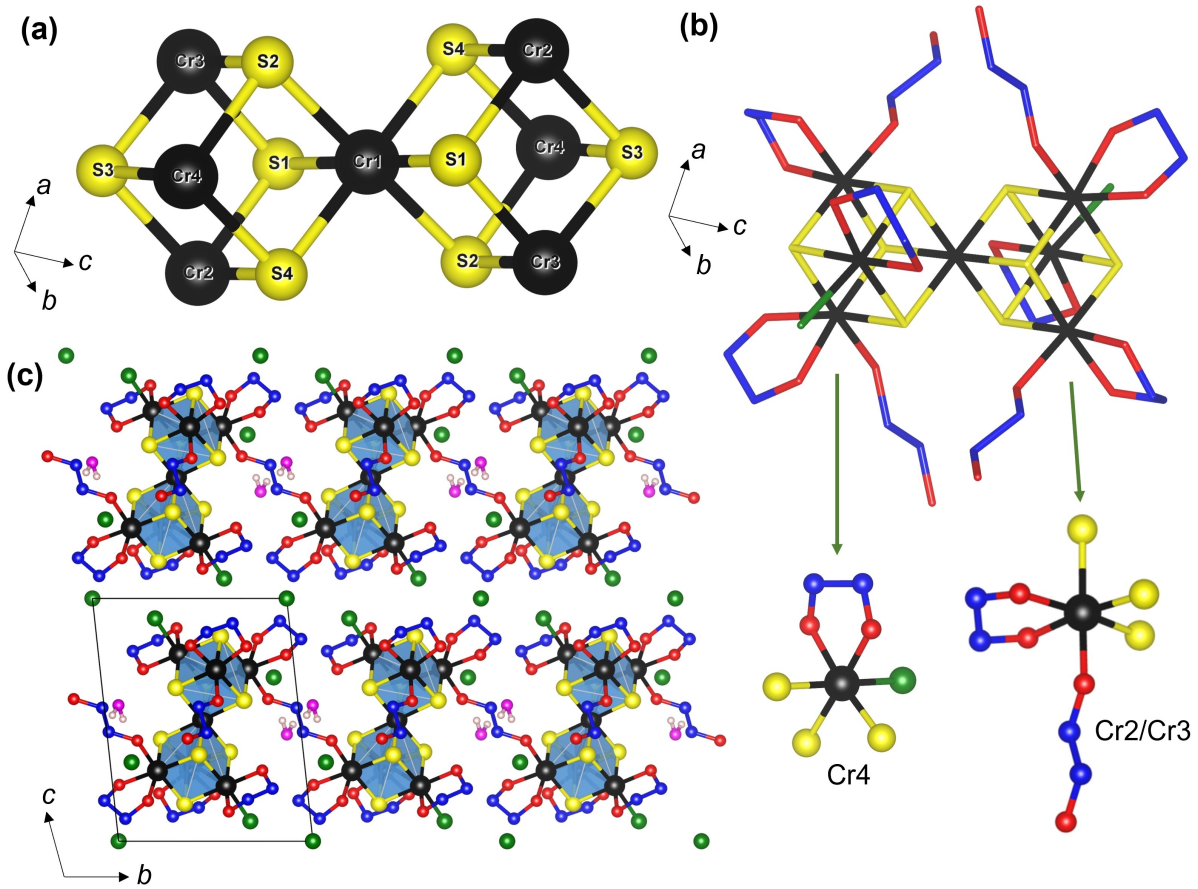

Figure 1. Crystal structure of $[Cr_7S_8(en)_8Cl_2]Cl_3\cdot 2H_2O$. **(a)** General view of a $[Cr_7S_8]^{5+}$ double-cube unit. **(b)** Stick model of a $[Cr_7S_8(en)_8Cl_2]^{3+}$ molecular unit showing the coordination environments around Cr atoms. **(c)** Overall structural view along [100] direction with the unit cell shown in black. Cr: black; S: yellow; N: red; C: blue; O: magenta; H: white. H atoms of ethylenediamine omitted for clarity.

batch of crystals. Under an applied field of 1000 Oe, temperature-dependent magnetic susceptibility (χ) showed paramagnetic behavior with no magnetic ordering down to 1.8 K (Figure S4). The χT product decreased gradually upon cooling from 300 K, reaching a plateau of ~1.8 emu·K mol^{-1} below 25 K and further decreasing at lower temperatures (Figure 2a). The $1/\chi$ vs. T dependence in the range of 100–300 K (Figure 2a, inset) was fit to the Curie-Weiss law ($R^2 = 0.9988$), $1/\chi = (T-\theta)/C$, yielding a large negative Weiss constant, $\theta = -224(2)$ K, that indicates strong AFM interactions between the Cr^{3+} centers. The fit resulted in a Curie constant $C = 13.68(8)$ emu·K mol^{-1} per formula unit, or 1.95(1) emu·K mol^{-1} per Cr^{3+} ion ($\mu_{eff} = 3.95(2)\ \mu_B$), which is only slightly higher than the value of 1.875 emu·K mol^{-1} ($\mu_{eff} = 3.87\ \mu_B$) expected for the $S = 3/2$ magnetic center.

The system of seven magnetically coupled $S = 3/2$ centers leads to $(2S+1)^7 = 16384$ microstates, which is very challenging to fit analytically. Therefore, the Magpack software[38] was used to simulate the magnetic behavior of $[Cr_7S_8(en)_8Cl_2]Cl_3 \cdot 2H_2O$. The system was modeled with the Hamiltonian that contains two magnetic exchange constants [Eq. (1)]:

$$\hat{\mathcal{H}} = g\mu_B \sum_{i=1}^{7} \hat{S}_i \vec{B}_z - 2J_1 \hat{S}_1 \sum_{i=2}^{7} \hat{S}_i - 2J_2 (\hat{S}_2\hat{S}_3 + \hat{S}_2\hat{S}_4 + \hat{S}_3\hat{S}_4 + \hat{S}_5\hat{S}_6 + \hat{S}_5\hat{S}_7 + \hat{S}_6\hat{S}_7) \quad (1)$$

where $\vec{B}_z$ is the applied magnetic field, $\hat{S}_i$ are the spin operators describing each of the Cr^{3+} centers (Figure 2b, inset): J_1 is the exchange constant corresponding to the magnetic coupling between the shared central Cr1 atom and the outlying Cr atoms, and J_2 is the exchange constant corresponding to the magnetic coupling within the Cr triangles on the opposite sides of the dicubane units. For the sake of simplicity, we have ignored the next-nearest neighbor interactions between the opposite triangles. Based on the value of $C = 1.95$ emu·K/mol and given that $C = g^2S(S+1)/8$, the Lande g-factor was fixed at 2.04. The best simulation of the experimental data was obtained with $J_1 = -20.0\ cm^{-1}$ and $J_2 = -21.0\ cm^{-1}$ (the simulation is shown with the solid red line in Figure 2a).

The field-dependent magnetization measurement performed at 300 K showed a steady linear increase producing a highest value of 0.25 μ_B at 7 T (Figure S5). However, a non-linear behavior is displayed at 1.8 K and the saturation magnetization reaches the value of 3 μ_B (Figure 2b), suggesting that the ground state of the system corresponds to the total spin of $S_T = 3/2$. In agreement with this observation, the χT vs. T curve plateaus to ~1.8 emu·K mol^{-1} below 25 K (Figure 2a), which is also close to the spin-only χT value of 1.875 emu·K mol^{-1} expected for $S_T = 3/2$.

Previously reported compounds containing isolated Cr dicubane clusters $[Cr_7S_8Cl_2(NH_3)_{14.5}(H_2O)_{1.5}]Cl_3 \cdot H_2O$[35] ($\mu_{eff} = 2.38\ \mu_B$) and $[Cr_7S_8(SCN)_4(NH_3)_{14}](SH)$[34] ($\mu_{eff} = 3.59\ \mu_B$) show similar trends in the temperature dependence of χT and $1/\chi$, but with smaller Weiss constants, $\theta = -14.72$ K and -66 K respectively, signifying weaker AFM coupling between Cr centers. Even though magnetic susceptibility studies have been conducted for many transition metal dicubane compounds, spin correlation calculations on magnetic data have rarely been performed except for some copper containing clusters due to relative simplicity of the $S = 1/2$ system with $2^7 = 128$ microstates. Spin-projection calculations performed on $[\{Cu_3\text{-}(Hpz^{tBu})_6(\mu_3\text{-}X)(\mu_3\text{-}OH)_3\}_2Cu]X_6$ ($X = Cl^-$, Br^-, NO_3^-) with AFM super-exchange, resulted in exchange integrals (J) varying from $-16\ cm^{-1}$ ($g = 2.14$) to $-73\ cm^{-1}$ ($g = 2.22$) for $S = 1/2$ Cu(II) centers.[32] AFM exchange parameters as high as $-188.4\ cm^{-1}$ ($g = 2.15$) were obtained for hydroxo-chloride Cu dicubanes clusters in $[Cu_7(OH)_6Cl_2(pn)_6(H_2O)_2](C(CN)_3)_4Cl_2$ (pn = 1,3-diaminopropane).[31] On the other hand, fully-hydroxo bridged $Cu_7(OH)_8$ dicubane clusters in

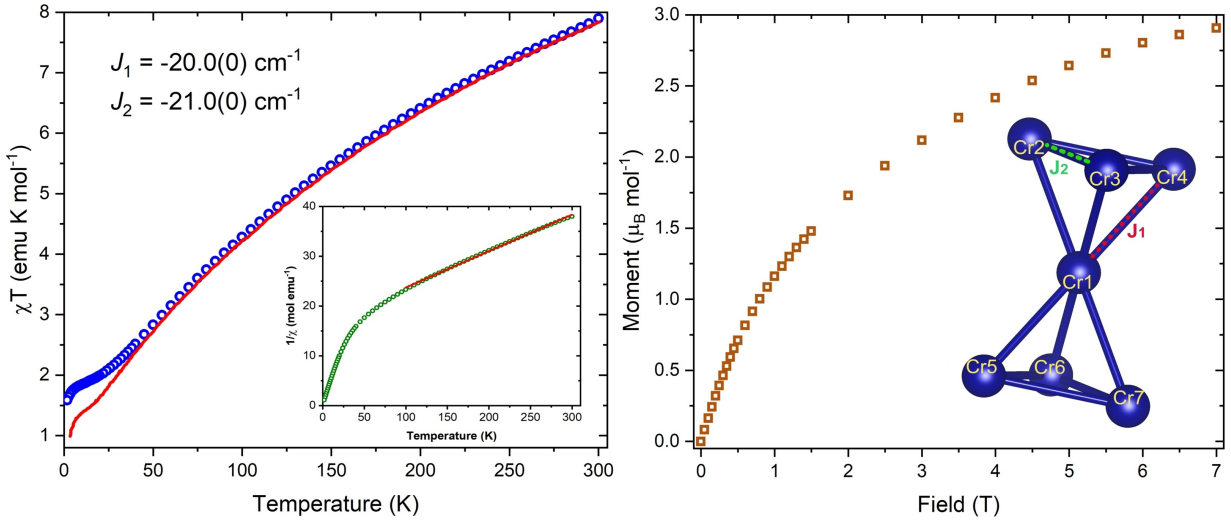

Figure 2. (a) The temperature dependence of χT and $1/\chi$ (inset) for $[Cr_7S_8(en)_8Cl_2]Cl_3 \cdot 2H_2O$. The solid red line in the main plot shows the best simulation of χT obtained with Magpack, while the solid red line in the inset shows the fit to the Curie-Weiss law in the 100–300 K region, $R^2 = 0.9988$. (b) The field dependence of magnetization measured at 1.8 K. The inset shows the numbering of Cr centers and the J_1 and J_2 exchange coupling constants defined in Equation (1).

$[Cu_2(bpym)_2(H_2O)_2(OH)_2](NO_3)_2 \cdot 4H_2O$ (*bpym* = 2,2′-bipyrimidine) showed FM interactions as indicated by positive fit values calculated for exchange parameters, $J = 0.4–5.4\ cm^{-1}$ ($g = 2.22$).[33] These examples demonstrate that not only the nature of the transition metal but also the ligands forming dicubanes are important for the magnetic interactions in such clusters.

Computational approach

Collinear DFT methods were used to calculate the total energy of various inequivalent spin configurations for the $S = 3/2$ Cr^{3+} centers, assuming a zero orbital momentum ($L = 0$). The Heisenberg Hamiltonian given in Equation (1) was used to obtain the J_1 and J_2 magnetic exchange constants. The DFT-calculated J_1 and J_2 values (-21.4 and $-30.2\ cm^{-1}$, respectively) are more negative than the values used in the Magpack simulation to provide the best fit to the experimental data (-20.0 and $-21.0\ cm^{-1}$, respectively, Figure S6). Nevertheless, in both cases the absolute magnitude of J_2 exceeds that of J_1. The calculated values reproduce the low-temperature plateau observed in the experimental χT vs. T curve, although the dependence simulated with the calculated J_1 and J_2 parameters shows systematically lower χT values, in agreement with the slightly stronger AFM coupling predicted by the theoretical model (Figure 3). Average distance corresponding to J_1 coupling between central and peripheral Cr atoms is 3.396 Å, while the average distance in the peripheral Cr_3 triangle, which corresponds to J_2 coupling, is 3.353 Å. The coupling between closer atoms is expected to be stronger and the difference in the Cr-Cr distances explains why $|J_1|$ is lower than $|J_2|$ in both experimental fitting and computations. The computations were performed for spin-spin coupling only omitting spin-orbit contribution which may explain the disagreement in the absolute computed and experimental values of the coupling constants.

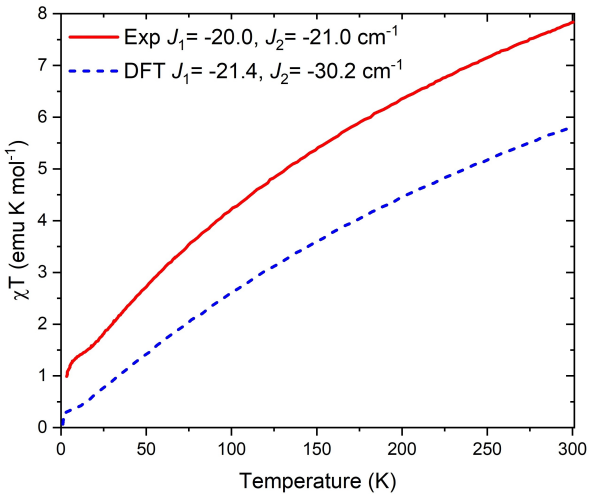

Figure 3. The temperature dependence of χT for the Cr_7 dicubane cluster simulated with the values of the magnetic exchange constants obtained from the DFT calculations (dashed blue line) and from the best simulation of the experimental data with Magpack (solid red line).

Using non-collinear magnetic DFT methods[51] including spin-orbit coupling, we calculated the local magnetic anisotropy of the central Cr^{3+} ion and the peripheral Cr^{3+} ions in the base triangles. The calculations show the easy axis being oriented along the direction connecting the center Cr atom and the two centers of the cubes. The calculated data were fit to the expression $H_{center} = DS_z^2 - E\left(S_x^2 - S_y^2\right)$, yielding $D = -67.3\ cm^{-1}$ and $E = 0.10\ cm^{-1}$ for the central Cr^{3+} ion and $D = -30.2\ cm^{-1}$ and $E = 0.73\ cm^{-1}$ for the basal Cr^{3+} ions. Somewhat unexpectedly, the calculations suggest substantial single-ion anisotropy at the $S = 3/2$ Cr^{3+} ions. This finding might be justified by the presence of the easy-axis direction coinciding with the shared body diagonal of the two cubane units. Verifying this prediction, however, requires a detailed investigation of $[Cr_7S_8(en)_8Cl_2]Cl_3 \cdot 2H_2O$ by advanced electron magnetic resonance methods..

Conclusions

In summary, we have developed a one-step solvothermal route to a polymeric dicubane cluster compound, $[Cr_7S_8(en)_8Cl_2]Cl_3 \cdot 2H_2O$ with $[Cr_7S_8(en)_8Cl_2]^{3+}$ cationic units and charge balancing Cl^- anions. The accompanying water molecules help in packing the overall structure and aided in crystal growth. The source of sulfur for the synthesis was DMSO and hence the use of additional reducing agents was not required. With regard to the magnetic properties, the Cr_7S_8 dicubane cluster shows strong magnetic frustration due to competing AFM exchange interactions between the central and peripheral Cr^{3+} ions. Curie Weiss fit on inverse magnetic susceptibility gives a highly negative Weiss temperature suggesting strong AFM interactions within the dicubane cluster. Magpack simulations performed on magnetic data as well as collinear DFT calculations result in negative exchange parameters confirming the AFM nature of the magnetic coupling between Cr atoms. The outcome of the DFT calculations recorded an absolute value of J_2 exceeding that of J_1, in agreement with the simulation of experimental data and average Cr–Cr distances in the cluster. The two couplings are of the same order of magnitude. Since the DFT calculations included only spin-spin coupling effects, without spin-orbital coupling, it is likely that the use of the simpler model led to the slight deviation from the experimentally simulated J values.

A potential development of this study can be connecting these clusters into a polymeric framework by means of covalent bonding. Ethylenediamine is a weak ligand for the magnetic exchange, and clusters bridged by such ligands are expected to show paramagnetic behavior. Nevertheless, one can envision that the use of conjugated bi- and tri-dentate ligands, especially organic radicals, may lead to structures where Cr_7S_8 dicubane clusters act as magnetically coupled superatoms.[52–56] A few examples of arranging the dicubane clusters into polymers were reported, such as polymers made from heptanuclear

$Co_7(\mu_3\text{-}OH)_8$ clusters coordinated by oxalate and piperazine ligands.[20] Such a polymeric system exhibits AFM ordering (T_N = 26 K) with a surprisingly low Weiss constant, $\theta = -2.76$ K, which is indicative of a FM contribution to magnetic susceptibility. Efforts to create such polymeric frameworks of linked dicubane clusters are currently underway.

Supporting Information

Table with Cr–N distances, crystallographic file (CIF), additional powder X-ray diffraction figures, SEM images, χ vs. T plot and, the Magpack simulations of the χT vs. T curve for $[Cr_7S_8(en)_8Cl_2]Cl_3 \cdot 2H_2O$.

Author Contributions

The manuscript was written through contributions of all authors.

Funding Sources

This research was supported by National Science Foundation DMR-2003783 grant to KK. *In-situ* decomposition experiments used the resources at the beamline 17-BM Advanced Photon Source, a U.S. Department of Energy (DOE) Office of Science User Facility operated for the DOE Office of Science by Argonne National Laboratory under Contract No. DE-AC02-06CH11357. Magnetic characterization and theoretical studies were performed as part of the Center for Molecular Magnetic Quantum Materials, an Energy Frontier Research Center funded by the U.S. Department of Energy, Office of Science, Basic Energy Sciences under Award no. DESC0019330.

Acknowledgements

The authors are thankful to Dr. Warren Straszheim, Dr. Shannon Lee, and Gayatri Viswanathan for the help with SEM/EDS data collection at MARL ISU and Dr. Wenqian Xu and Dr. Andrey Yakovenko (APS ANL) for help with collecting *in-situ* synchrotron XRD patterns.

Conflict of Interest

Authors declare no conflict of interests.

Data Availability Statement

The data that support the findings of this study are available from the corresponding author upon reasonable request.

Keywords: antiferromagnetic coupling · crystal structures · dicubane clusters · magnetic frustration · solvothermal synthesis

[1] J. Beck, *Coord. Chem. Rev.* **1997**, *163*, 55–70.
[2] E. Ahmed, M. Ruck, *Coord. Chem. Rev.* **2011**, *255*, 2892–2903.
[3] A. Stephenson, M. D. Ward, *Dalton Trans.* **2011**, *40*, 10360–10369.
[4] A. M. Najar, I. S. Tidmarsh, H. Adams, M. D. Ward, *Inorg. Chem.* **2009**, *48*, 11871–11881.
[5] V. W.-W. Yam, E. C.-C. Cheng, N. Zhu, *Angew. Chem. Int. Ed.* **2001**, *40*, 1763–1765; *Angew. Chem.* **2001**, *113*, 1813–1815.
[6] D. Casanova, M. Llunell, P. Alemany, S. Alvarez, *Chem. Eur. J.* **2005**, *11*, 1479–1494.
[7] K. C. Kumara Swamy, R. O. Day, R. R. Holmes, *J. Am. Chem. Soc.* **1987**, *109*, 5546–5548.
[8] R. R. Holmes, K. C. Kumara Swamy, C. G. Schmid, R. O. Day, *J. Am. Chem. Soc.* **1988**, *110*, 7060–7066.
[9] R. Chakrabarty, S. J. Bora, B. K. Das, *Inorg. Chem.* **2007**, *46*, 9450–9462.
[10] G. F. Swiegers, J. K. Clegg, R. Stranger, *Chem. Sci.* **2011**, *2*, 2254–2262.
[11] S. Z. Knottenbelt, J. E. McGrady, *J. Am. Chem. Soc.* **2003**, *125*, 9846–9852.
[12] L. Noodleman, J. G. Norman, J. H. Osborne, A. Aizman, D. A. Case, *J. Am. Chem. Soc.* **1985**, *107*, 3418–3426.
[13] S. Sharma, K. Sivalingam, F. Neese, G. K.-L. Chan, *Nat. Chem.* **2014**, *6*, 927–933.
[14] S. C. Lee, W. Lo, R. H. Holm, *Chem. Rev.* **2014**, *114*, 3579–3600.
[15] Y. Shim, B. D. Yuhas, S. M. Dyar, A. L. Smeigh, A. P. Douvalis, M. R. Wasielewski, M. G. Kanatzidis, *J. Am. Chem. Soc.* **2013**, *135*, 2330–2337.
[16] Y. Shim, R. M. Young, A. P. Douvalis, S. M. Dyar, B. D. Yuhas, T. Bakas, M. R. Wasielewski, M. G. Kanatzidis, *J. Am. Chem. Soc.* **2014**, *136*, 13371–13380.
[17] J. Tercero, E. Ruiz, S. Alvarez, A. Rodríguez-Fortea, P. Alemany, *J. Mater. Chem.* **2006**, *16*, 2729–2735.
[18] J. M. Clemente-Juan, C. Mackiewicz, M. Verelst, F. Dahan, A. Bousseksou, Y. Sanakis, J.-P. Tuchagues, *Inorg. Chem.* **2002**, *41*, 1478–1491.
[19] A. Das, F. J. Klinke, S. Demeshko, S. Meyer, S. Dechert, F. Meyer, *Inorg. Chem.* **2012**, *51*, 8141–8149.
[20] R.-K. Chiang, C.-C. Huang, C.-S. Wur, *Inorg. Chem.* **2001**, *40*, 3237–3239.
[21] A. Eich, S. Schlüter, G. Schnakenburg, J. Beck, *Z. Anorg. Allg. Chem.* **2013**, *639*, 375–383.
[22] Q. Zhang, I. Chung, J. I. Jang, J. B. Ketterson, M. G. Kanatzidis, *J. Am. Chem. Soc.* **2009**, *131*, 9896–9897.
[23] E. Ahmed, J. Breternitz, M. F. Groh, A. Isaeva, M. Ruck, *Eur. J. Inorg. Chem.* **2014**, 3037–3042.
[24] R. A. Hussain, H. Kamarudin, S. Auluck, I. V. Kityk, *J. Phys. Chem. B* **2011**, *115*, 11763–11769.
[25] K. C. Kumara Swamy, R. O. Day, R. R. Holmes, *J. Am. Chem. Soc.* **1988**, *110*, 7543–7544.
[26] R. Hernandez-Molina, V. P. Fedin, M. N. Sokolov, D. M. Saysell, A. G. Sykes, *Inorg. Chem.* **1998**, *37*, 4328–4334.
[27] R. Hernandez-Molina, A. J. Edwards, W. Clegg, A. G. Sykes, *Inorg. Chem.* **1998**, *37*, 2989–2994.
[28] D. M. Saysell, M. N. Sokolov, A. G. Sykes, In *Transition Metal Sulfur Chemistry*, (Eds: E. I. Stiefel, K. Matsumoto), American Chemical Society, Washington, DC, **1996**, p. 216.
[29] D. M. Saysell, A. G. Sykes, *Inorg. Chem.* **1996**, *35*, 5536–5539.
[30] R. Hernandez-Molina, M. N. Sokolov, A. G. Sykes, *Acc. Chem. Res.* **2000**, *34*, 223–230.
[31] X. Liu, J. A. McAllister, M. P. de Miranda, E. J. L. McInnes, C. A. Kilner, M. A. Halcrow, *Chem. Eur. J.* **2004**, *10*, 1827–1837.
[32] S. Triki, F. Thétiot, J. S. Pala, S. Golhen, J. M. Clemente-Juan, C. J. Gómez-García, E. Coronado, *Chem. Commun.* **2001**, 2172–2173.
[33] J. A. Real, G. De Munno, R. Chiappetta, M. Julve, F. Lloret, Y. Journaux, J. Colin, G. Blondin, *Angew. Chem. Int. Ed.* **1994**, *33*, 1184–1186; *Angew. Chem.* **1994**, *106*, 1223–1225.
[34] J. Yang, P. Jiang, Z. Zhou, M. Yue, D. Yang, S. Chen, T. Yang, *Cryst. Growth Des.* **2019**, *19*, 6028–6032.
[35] K.-Z. Du, M.-L. Feng, J.-R. Li, X.-Y. Huang, *CrystEngComm.* **2013**, *15*, 5594–5597.
[36] G. M. Sheldrick, *Acta Crystallogr. Sect. A* **2008**, *64*, 112–122.
[37] G. M. Sheldrick, *Acta Crystallogr. Sect. C Struct. Chem.* **2015**, *71*, 3–8.
[38] J. J. Borrás-Almenar, J. M. Clemente-Juan, E. Coronado, B. S. Tsukerblat, *J. Comput. Chem.* **2001**, *22*, 985–991.
[39] G. Kresse, J. Furthmüller, *Phys. Rev. B* **1996**, *54*, 11169.
[40] G. Kresse, J. Furthmüller, *Comput. Mater. Sci.* **1996**, *6*, 15–50.
[41] W. Kohn, L. J. Sham, *Phys. Rev.* **1965**, *140*, A1133.

[42] P. E. Blöchl, *Phys. Rev. B* **1994**, *50*, 17953.
[43] J. P. Perdew, K. Burke, M. Ernzerhof, *Phys. Rev. Lett.* **1996**, *77*, 3865.
[44] T. Diao, P. White, I. Guzei, S. S. Stahl, *Inorg. Chem.* **2012**, *51*, 11898–11909.
[45] J. H. Price, A. N. Williamson, R. F. Schramm, B. B. Wayland, *Inorg. Chem.* **2002**, *11*, 1280–1284.
[46] F. A. Cotton, E. V. Dikarev, M. A. Petrukhina, S.-E. Stiriba, *Inorg. Chem.* **2000**, *39*, 1748–1754.
[47] E. V. Dikarev, M. A. Petrukhina, X. Li, E. Block, *Inorg. Chem.* **2003**, *42*, 1966–1972.
[48] S. I. Levchenkov, I. N. Shcherbakov, L. D. Popov, V. G. Vlasenko, K. Y. Suponitskii, A. A. Tsaturyan, V. V. Lukov, V. A. Kogan, *Russ. J. Coord. Chem.* **2014**, *40*, 523–530.
[49] M. Wu, J. Rhee, T. J. Emge, H. Yao, J. H. Cheng, S. Thiagarajan, M. Croft, R. Yang, J. Li, *Chem. Commun.* **2010**, *46*, 1649–1651.
[50] J. Li, Z. Chen, R.-J. Wang, D. M. Proserpio, *Coord. Chem. Rev.* **1999**, 707–735.
[51] J. Kubler, K.-H. Hock, J. Sticht, A. R. Williams, *J. Phys. F* **1988**, *18*, 469–483.
[52] Z. Luo, A. W. Castleman, *Acc. Chem. Res.* **2014**, *47*, 2931–2940.
[53] A. M. Champsaur, A. Velian, D. W. Paley, B. Choi, X. Roy, M. L. Steigerwald, C. Nuckolls, *Nano Lett.* **2016**, *16*, 5273–5277.
[54] S. A. Claridge, A. W. Castleman, S. N. Khanna, C. B. Murray, A. Sen, P. S. Weiss, *ACS Nano* **2009**, *3*, 244–255.
[55] M. Qian, A. C. Reber, A. Ugrinov, N. K. Chaki, S. Mandal, H. M. Saavedra, S. N. Khanna, A. Sen, P. S. Weiss, *ACS Nano* **2010**, *4*, 235–240.
[56] S. N. Khanna, P. Jena, *Phys. Rev. B* **1995**, *51*, 13705.

Manuscript received: October 18, 2021
Accepted manuscript online: November 10, 2021
Version of record online: December 13, 2021